

Continuous measurement of a microwave-driven solid state qubit

S. D. Barrett^{1,*} and T. M. Stace^{2,†}

¹Hewlett-Packard Laboratories, Filton Road, Stoke Gifford, Bristol BS34 8QZ, U.K.

²DAMTP, University of Cambridge, Wilberforce Road, CB3 0WA, U.K.

(Dated: March 23, 2022)

We analyze the dynamics of a continuously observed, damped, microwave-driven solid state charge qubit. The qubit consists of a single electron in a double well potential, coupled to an oscillating electric field, and which is continuously observed by a nearby point contact electrometer. The microwave field induces transitions between the qubit eigenstates, which have a profound effect on the detector output current. We show that useful information about the qubit dynamics, such as dephasing and relaxation rates, and the Rabi frequency, can be extracted from the DC detector conductance and the detector output noise power spectrum. We also demonstrate that these phenomena can be used for single shot electron spin readout, for spin based quantum information processing.

PACS numbers: 78.70.Gq, 42.50.Lc, 03.67.Lx, 63.20.Kr

Recently, rapid experimental progress in mesoscopic physics has meant that it is now possible to confine, manipulate, and measure small numbers of electrons in single or coupled quantum dots [1, 2, 3, 4]. The mesoscopic environment of such confined electron systems may consist of phonons, electrons, and other electromagnetic degrees of freedom. Thus these experiments are particularly interesting as they allow the complex interaction between such confined systems and their environment to be studied at the single electron level. Furthermore, in view of the potential applications of such systems in solid state quantum information processing [5], understanding these interactions is important, as it allows qubit decoherence mechanisms to be studied and accurately characterised.

Of particular interest are coupled quantum dot (CQD) qubit systems driven by oscillating electric fields. The presence of a driving field resonant to the qubit energy splitting can drive transitions into the excited state. Continuous measurement of such systems can reveal important spectroscopic information about the qubit, such as the qubit splitting, Rabi frequency, and decoherence rates. Earlier work has focussed on current transport through driven, open CQD systems [6, 7]. In a recent experiment, a driven qubit comprising a single electron in a closed CQD system was continuously observed via a nearby quantum point contact (QPC) detector [4].

In this Letter, we theoretically analyse this system (see Fig. 1). We account for the coupling of the CQD both to the QPC and to a generic bosonic environment, which may comprise of phonons or other electromagnetic degrees of freedom [8]. Both the detector and the environment contribute to the qubit relaxation and dephasing rates. We also demonstrate how resonant driving phenomena can be used for single-shot readout of the electron spin. Our results are also relevant to other driven qubit systems, e.g. superconducting charge qubits [9, 10].

A number of authors have considered the continuous measurement of undriven charge qubit systems by a QPC detector [11, 12, 13]. Continuous measurement of driven

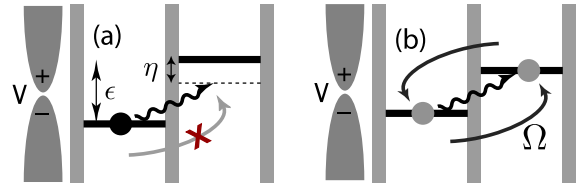


FIG. 1: Schematic of a CQD charge qubit measured by a QPC under (a) non-resonant and (b) resonant microwave driving.

superconducting flux qubits has also been considered [14]. In what follows, we adopt the quantum trajectories description of the measurement process [12, 13, 15], and generalize results obtained in previous work [16, 17] on the measurement of undriven charge qubits using a QPC at arbitrary bias voltage. We first derive a master equation (ME) for the dynamics of the damped, driven charge qubit system. We use solutions of the ME to determine the DC conductance and current power spectra of the QPC detector, and show how various qubit parameters can be extracted from measurements of these quantities. Finally, we describe our technique for spin readout.

The model system we consider is shown in Fig. 1, for which the total Hamiltonian is given by $H = H_{\text{sys}} + H_{\text{drive}} + H_{\text{meas}} + H_{\text{leads}} + H_{\text{sb}} + H_{\text{env}}$, where ($\hbar = 1$)

$$H_{\text{sys}} = \begin{pmatrix} \epsilon_x & \epsilon_z \end{pmatrix} = 2 \begin{pmatrix} \epsilon_x^{(e)} & \epsilon_z^{(e)} \end{pmatrix}; \quad (1)$$

$$H_{\text{drive}} = \sum_k \cos[(\epsilon_x - \epsilon_z)t] (\cos \epsilon_z + \sin \epsilon_x); \quad (2)$$

$$H_{\text{meas}} = (T + \epsilon_z) a_{D,q}^\dagger a_{S,q} + H.c.; \quad (3)$$

$$H_{\text{leads}} = \sum_{k,q} \epsilon_{S,q} a_{S,q}^\dagger a_{S,q} + \sum_{q} \epsilon_{D,q} a_{D,q}^\dagger a_{D,q}; \quad (4)$$

$$H_{\text{sb}} = \sum_i \epsilon_i (b_i^\dagger + b_i); \quad H_{\text{env}} = \sum_i \epsilon_i b_i^\dagger b_i; \quad (5)$$

Here, H_{sys} is the bare qubit Hamiltonian, in which $\epsilon_x = \frac{1}{2}(\epsilon_{lhr} + \epsilon_{rhl})$ and $\epsilon_z = \frac{1}{2}(\epsilon_{lhl} - \epsilon_{rhr})$, where $\epsilon_{l/r}$ ($\epsilon_{l/r}$) denotes an electron state localized on the left (right) dot, $\epsilon = \frac{\epsilon_x^2 + \epsilon_z^2}{2}$ is the qubit energy splitting, and

$\hat{H}_z^{(e)} = \hbar g_z \hat{\sigma}_z$, \hat{H}_{drive} corresponds to the driving field with frequency $\omega_0 = \omega_z + \omega_x$, which may couple to both the $\hat{\sigma}_x$ and $\hat{\sigma}_z$ qubit operators, as parameterized by \hat{H}_{meas} denotes the qubit-detector coupling, in terms of the dimensionless tunnelling parameters $T = \frac{\hbar}{2 g_S g_D} T$ and $\Delta = \frac{\hbar}{2 g_S g_D} \Delta$, and $\omega_0 = \frac{\omega_z + \omega_x}{2}$. We have assumed that the tunnelling amplitudes, T and Δ , and the densities of lead modes, g_S and g_D , are approximately independent of k and q over the energy range where tunnelling is allowed. H_{leads} is the free Hamiltonian of the source and drain leads, where $a_{S,j}$ ($a_{D,j}$) is the annihilation operator for an electron in the j th source (drain) mode. H_{sb} and H_{env} correspond to a standard spin-boson coupling to a generic bath of bosons [18], where b_i is the annihilation for the i th boson mode.

To simplify the Hamiltonian, we first transform to an interaction picture defined by $H_0 = \hbar \omega_z \hat{\sigma}_z = 2\hbar + H_{\text{leads}} + H_{\text{env}}$, and make our first rotating wave approximation (RWA) and neglect terms oscillating rapidly compared to ω_0 and the microwave detuning, $\omega_0 - \omega_z$. Under this transformation, the time dependence is transferred to the interaction term and the Hamiltonian becomes

$$H_I(t) = \frac{\hbar}{2} \hat{\sigma}_z^{(e)} \hat{\sigma}_x^{(e)} + A_I(t) \hat{Y}(t) + B_I(t) \hat{Z}(t); \quad (6)$$

where $\hat{\sigma}_x^{(e)} = \sin(\frac{\omega_0}{2}) \hat{\sigma}_x$. We have defined the system operators $A_I(t) = \sum_n e^{i\omega_n t} P_n$ and $B_I(t) = \sum_n e^{i\omega_n t} Q_n$, with $\omega_n = 0$; $\omega_0, P_1 = T + \cos(\frac{\omega_z}{2})$, $P_2 = P_3 = \frac{1}{2} \sin(\frac{\omega_z}{2})$, $Q = \cos(\frac{\omega_z}{2})$, and $Q_2 = Q_3 = \frac{1}{2} \sin(\frac{\omega_z}{2})$. We have also defined the operators $Y(t) = \sum_{k,q} e^{i(\omega_{S,k} - \omega_{D,q})t} a_{D,q}^\dagger a_{S,k} + H.c.$ and $Z(t) = \sum_{i,j} e^{i(\omega_{B,i} - \omega_{D,j})t} b_i^\dagger + H.c.$ which act on the QPC and bosonic environment degrees of freedom, respectively.

To derive the ME for the dynamics of the qubit alone, we further transform to a frame defined by $H_0' = \frac{\hbar}{2} \hat{\sigma}_z^{(e)} - \frac{\hbar}{2} \hat{\sigma}_x^{(e)}$, in which all the dynamics are contained in the qubit-QPC and qubit-environment interaction terms. Then $H_I'(t) = A_I'(t) \hat{Y}(t) + B_I'(t) \hat{Z}(t)$, where $A_I'(t) = \sum_{nn'} e^{i(\omega_{nn'} + \omega_n^0)t} P_{nn'}$ and $B_I'(t) = \sum_{nn'} e^{i(\omega_{nn'} + \omega_n^0)t} Q_{nn'}$, for some operators $P_{nn'}$ and $Q_{nn'}$, and $\omega_n^0 = 0$; $\omega_0^0 = \frac{\omega_0}{2} + \frac{\omega_z}{2}$. In this picture, the qubit density matrix, ρ , satisfies

$$\dot{\rho}(t) = -\text{Tr}_{\text{B,D}} \int_0^t dt' [H_I'(t); [H_I'(t'); \rho(t')]] \rho(t); \quad (7)$$

We now make a Born-Markov approximation, setting the lower limit of the integral to -1 and $\rho(t) = \rho^0(t) + \delta \rho(t)$, where ρ^0 , $\delta \rho$, and ρ_B are equilibrium density matrices for the source, drain, and bath degrees of freedom. At this point, it is convenient to introduce the asymmetric quantum noise power spectra [19, 20] for the QPC and bath, $S_Y(\omega) = \frac{1}{R_1} \int_{-1}^0 dt e^{i\omega t} \text{Tr}[\dot{Y}(t) Y(0) \rho_S \rho_D] = (\omega - \omega_0) + (\omega + \omega_0)$ and $S_Z(\omega) = \frac{1}{R_1} \int_{-1}^0 dt e^{i\omega t} \text{Tr}[\dot{Z}(t) Z(0) \rho_B] = 2 J(\omega) [1 +$

$n(\omega)] + 2 J(\omega) n(\omega)$, where $\omega = (\omega + \omega_0)/2$ is the ramp function, eV_D is the source-drain bias across the detector, $J(\omega) = \frac{1}{\pi} \frac{\omega^2}{\omega^2 + \gamma_D^2}$ is the bath spectral density, and $n(\omega)$ is the thermal equilibrium Bose occupation number. To proceed, we make a second RWA, where we neglect terms in Eq.(7) rotating at a rate ω_0 . This RWA is justified in the limit of weak coupling to the detector and environment, $\omega_0 \ll S_{Y,Z}(\omega_n)$ [26]. We also assume that the driving field is sufficiently weak that $S_{Y,Z}(\omega_n + \omega_n^0) \approx S_{Y,Z}(\omega_n)$, i.e. that the noise spectra are slowly varying over frequencies of order ω_0 . Finally, in order to treat dephasing within our perturbative technique, we require that $\lim_{\omega \rightarrow 0} J(\omega) / \omega^s$ where $s > 1$, i.e. that the bath is ohmic or superohmic at low frequencies.

These approximations allow us to derive a ME which is valid for arbitrary source-drain bias and arbitrary bath temperature. However, in this Letter, we restrict our attention to the low bias ($eV < \dots$) and low temperature ($kT \ll \dots$) regime, which has been probed in a recent [4]. In this case, the master equation for the qubit in the original interaction picture is given by

$$\dot{\rho}(t) = -i \left[\frac{\hbar}{2} \hat{\sigma}_z^{(e)} \hat{\sigma}_x^{(e)}; \rho(t) \right] + \frac{1}{2} \gamma_D [S_Y(\omega)] \rho(t) + \gamma_D [S_Z(\omega)] \rho(t) - \Gamma \rho(t); \quad (8)$$

where $\gamma = \gamma_D^{\text{det}} + \gamma_D^{\text{env}}$ is the pure dephasing rate, with $\gamma_D^{\text{det}} = 2 \cos^2 S_Y(0)$ and $\gamma_D^{\text{env}} = 2 \cos^2 S_Z(0)$. $\gamma_r = \gamma_r^{\text{det}} + \gamma_r^{\text{env}}$ is the relaxation rate, with $\gamma_r^{\text{det}} = 2 \cos^2 S_Y(\omega)$ and $\gamma_r^{\text{env}} = \cos^2 S_Z(\omega)$. We have also defined $D[A] = A^\dagger A - (A^\dagger A + A^\dagger A)/2$.

DC conductance The DC current through the QPC is related to the steady state occupation probability of the dot nearest the QPC, to first order in δ , by $I = 4 \hbar I_0$

$\hbar I_0$ where I_0 corresponds to the current when the electron is localized in state $|j\rangle$ and $I = 4$ TeV [16, 17]. Using Eq. (8), we can compute the steady state occupation of the left well, and the scaled conductance $M = 1 + (I - I_0)/I_0 = 1 - \hbar I_0$ is given by

$$M = \frac{1}{2} \frac{\gamma_r(\omega^2 + \omega_0^2)}{2[\gamma_r^2 + \gamma_0(\omega^2 + \gamma_r \omega_0)]}; \quad (9)$$

where $\gamma_0 = \gamma_r + \gamma_r = 2$ is the total dephasing rate. M is plotted as a function of ω in Fig. 2(a). Note that Fig. 2(a) is in excellent qualitative agreement with recent experimental observations [4, 9, 10]. The absence of multi-photon resonances in Fig. 2(a) is a consequence of the first RWA made above.

The resonances occur at $\omega = \omega_0^2$. Useful spectroscopic information may be extracted from these resonant peaks. If the driving frequency, ω_0 , is known, and the Rabi frequency, γ , is known independently (e.g. from observations of the time dependence of the detector current, as discussed below) then γ_r and γ_0 can both be

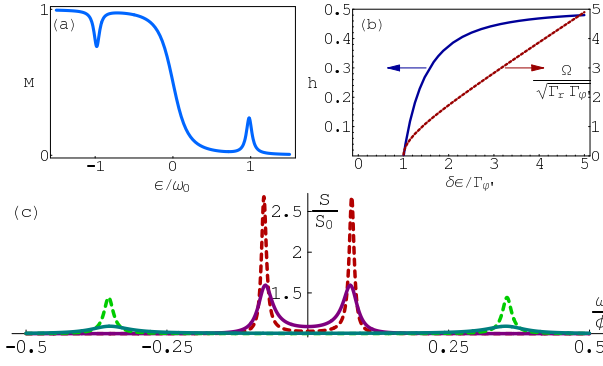


FIG. 2: (a) Variation in conductance (scaled between 0 and 1) versus dot bias. Parameters $\Gamma_r = \Gamma_l = 0.03\Gamma_0$ and $\Gamma_0 = 0.2\Gamma_0$ were taken to be constant over the entire range of ϵ . (b) The peak height h as a function of peak width $\delta\epsilon$. Increasing microwave power scans from left to right. Also shown is the relationship between h and the Rabi frequency Ω . (c) Power spectrum, $S(\Delta)$. Inner peaks: $\Delta = 20$, outer peaks: $\Delta = 4$. The tall peaks have detector limited dephasing, $\Gamma_r = \Gamma_l = 2^2 \text{ eV} \cos^2$, whilst the short peaks are dominated by phonon dephasing, $\Gamma_r = 0.03$. Other parameters are $eV = 0.5$, $\Gamma_r = 0.1$, $\Gamma_0 = 0.5$.

determined. When Γ_0 is small and assuming that Γ_r , Γ_l and Γ_0 do not vary significantly across the peak, from Eq. (9) we find $\Gamma_r \Gamma_l \Gamma_0 (2^2 - 2_0 - 1)$, where Γ_0 is the halfwidth-halfmaximum for the peak. Therefore, plotting h against $\delta\epsilon$ allows both Γ_r and Γ_l to be determined. However, in the absence of time-resolved measurements, Γ_0 may be unknown, because the relationship between the input microwave power and the electric field coupling to the qubit may be unknown. In this case, $\Gamma_r \Gamma_l$ can still be extracted by plotting the peak height, h , against $\delta\epsilon$, for different values of the incident power. Again assuming Γ_0 is small and that Γ_r , Γ_l and Γ_0 do not vary significantly across the peak, h and $\delta\epsilon$ are related by $h - 1 = 2\Gamma_r \Gamma_l \Gamma_0 \delta\epsilon^2$, which is independent of the (unknown) quantity Γ_0 . These results are shown in Figure 2(b). Note that, for sufficiently weak driving, the peak width directly gives $\Gamma_r \Gamma_l$, while for stronger driving, the peak width is proportional to Γ_0 .

Power Spectrum Further spectroscopic information may be obtained from the power spectrum of the current through the QPC, which is given by $S(\Delta) = 2^{-1} \text{d} G(\Delta) / \text{d} \Delta$, where $G(\Delta) = E[I(t + \Delta)I(t)] / E[I(t + \Delta)]E[I(t)]$, is the current autocorrelation function, and $E[\cdot]$ denotes the classical expectation. $S(\Delta)$ can be computed using the same formalism as in [13, 17]. In the low-bias regime the scaled (symmetric) power spectrum $S'(\Delta) = S(\Delta) - S_0$ (where $S_0 = 2eI_D C = e^2 T^2 \text{ eV}$ is the shot noise background) is closely approximated by

$$S'(\Delta) = \frac{S_0 \Gamma_0^2}{2_0 + (\Delta/\Gamma_0)^2} + \frac{S_0 \Gamma_0^2}{2_0 + (\Delta/\Gamma_0)^2} + \frac{S_0 \Gamma_0^2}{2_0 + \Delta^2} + 1; \quad (10)$$

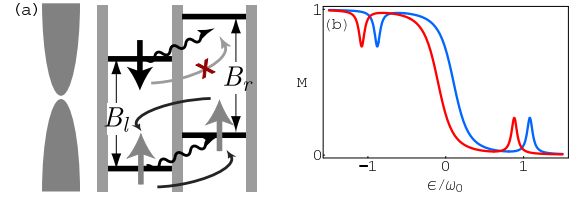


FIG. 3: (a) Schematic of spin measurement scheme. (b) Conductance curves for spin-up and spin-down configurations showing distinct resonance peaks.

where

$$\begin{aligned} \Gamma_0 &= \frac{2\Gamma_r^2 + \Gamma_l^2 + \Gamma_r^2 + 2\Gamma_r^2 + 3\Gamma_r^2}{4(\Gamma_r^2 + \Gamma_l^2)} \Gamma_r; \\ \Gamma_0 &= \frac{2\Gamma_r^2 + \Gamma_l^2 + \Gamma_r^2 + \Gamma_r^2}{2(\Gamma_r^2 + \Gamma_l^2)} \Gamma_r; \\ S_0 &= \frac{4\Gamma_r^2 \Gamma_l^2}{2(2\Gamma_r^2 + \Gamma_l^2) + (2\Gamma_r^2 + 3\Gamma_r^2) \Gamma_r}; \\ S_0 &= \frac{4\Gamma_r^2 \Gamma_l^2 \Gamma_0^2 (\Gamma_r^2 + 4(2\Gamma_r^2 + \Gamma_l^2) \Gamma_r + 4\Gamma_r^2 \Gamma_l^2)}{(2\Gamma_r^2 + \Gamma_l^2 + (2\Gamma_r^2 + \Gamma_l^2) \Gamma_r)^3}; \end{aligned}$$

Thus the positions of the peaks yield the Rabi frequency Γ_0 , while the widths of the peaks contain other important spectroscopic information about the qubit. The height of the peaks at $\Delta = 0$ is maximised when the external field is resonant with the qubit transition, $\Delta = 0$. Note that $S(\Delta) \leq 2$ and thus the peak heights are no more than three times the shot noise background, as shown in Fig. 2(c). The bound $S(\Delta) = 2$ can only be met when dephasing is detector dominated, since extra dephasing due to the environment reduces the height of the peaks.

Spin measurement Motivated by the preceding analysis, we propose a method for single shot spin readout, using a microwave driving field and an inhomogeneous Zeeman splitting across the CQD. This splitting could be generated by an inhomogeneous magnetic field, or engineering different g-factors in each dot. In this case, one spin configuration, say spin-down, may be made resonant with the driving field, whilst the other, spin-up, is detuned by an amount Δ , and thus the spin can be determined by observing the current through the QPC [Fig. 3(a)]. Such a scheme is analogous to the method of spin readout via quantum jumps in atomic systems [21]. We note that alternative methods for spin readout have also been proposed, via inhomogeneous fields but without driving [22], and by driving spin- $\frac{1}{2}$ transitions within a single dot [23].

Spin can be included in the Hamiltonian by replacing σ_x and σ_z in Eqs. (1-5) with generalized tunnelling and bias operators, i.e. $\sigma_x \rightarrow c_{1\#}^\dagger c_{2\#} + c_{1\#}^\dagger c_{2\#} + H.c.$ and $\sigma_z \rightarrow n_1 - n_2$ where $n_i = c_{i\#}^\dagger c_{i\#}$ denotes the number of electrons on site i . The inhomogeneous Zeeman splitting

is included by adding the term

$$H_{\text{Zeeman}} = \frac{1}{2} \sum_{i=1,2} B_i S_i^{(z)} \quad (11)$$

to H_{sys} , where B_i denotes the Zeeman splitting on each site, and $S_i^{(z)} = c_{i\uparrow}^\dagger c_{i\uparrow} - c_{i\downarrow}^\dagger c_{i\downarrow}$. We neglect any explicit coupling between spin up and spin down states (processes which can induce such transitions can be accounted for by a finite spin lifetime, which we discuss below).

The Zeeman term amounts to a spin dependent bias between the dots, $B_{\#} = (B_2 - B_1)/2$. The DC response of the detector is therefore shifted for each spin configuration, as shown in Fig. 3(b). If $B_{\#} \gg B_1$ & B_2 , the resonant peaks are clearly resolved. In this case, if ν is tuned such that the spin-down transition is resonant with the driving field, the currents for each spin configuration are approximately $I_{\#} \approx I_0$ and $I_{\#} \approx I_0 - I = 2$. If the detector is shot noise limited, the time taken to resolve these currents is $\tau_{\#} = (I_{\#}^{1=2} - I_{\#}^{1=2})^2 = 2e^2 \hbar / 32 I_0$. Thus $\tau_{\#} = 4 \tau_{01}$ where τ_{01} is the time taken to distinguish the currents due to 0 and 1 electrons on the dot adjacent to the QPC. It is believed that shot noise limited QPC detectors will be available in the near future with $\tau_{01} \approx 25$ ns [24], and so $\tau_{\#} \approx 100$ ns should be possible. This compares favourably with recently observed spin lifetimes ($\tau_1 \approx 1$ ms) in GaAs quantum dots [5].

The use of microwave driving for spin readout offers some advantages over other schemes where no driving is used. Firstly, a relatively small differential Zeeman splitting is needed. In order to clearly resolve the resonant peaks, we require $B_{\#} \gg B_1$ & B_2 . The lower bound on the peak width is given by $\Delta \nu > \nu_0$. So for a charge dephasing rate of $\nu_0 \approx 10^8$ s⁻¹ [2], we require $B_{\#} \gg B_1 \approx 0.07$ eV. If one attempts readout via an inhomogeneous Zeeman splitting but without driving [22], then to obtain a comparable signal-to-noise, the differential Zeeman splitting must be larger than the central transition region in Fig. 3(b), i.e. $B_{\#} \gg B_1 + \max(\hbar \nu, kT)$. For $T = 100$ mK, $B_{\#} \gg B_1 \approx 9$ eV is required. Thus in GaAs ($g = 0.44$), with a uniform field of 1 T, our scheme requires a g -factor variation between the dots of $g_{\#} = 0.3\%$, whereas without driving, one would require $g_{\#} = 35\%$.

Secondly, the scheme can be used in such a way that a definite signal is always obtained for both spin configurations. Switching the microwave frequency first on resonance with the spin-down transition, and then on resonance with the spin-up transition yields a definite signal indicating the spin state. That is, when the driving frequency is switched, the DC conductance will increase if the electron is spin-up, and will decrease if it is spin-down. This is in contrast to other measurement schemes in which a definite signal is only registered for one spin configuration, [22, 24, 25], with the other state indicated only by the lack of a signal. This has the advantage of eliminating false negative signals, where an "no-signal"

event is erroneously recorded as evidence for a particular spin configuration. Thus the resulting measurement fidelity should be improved.

In summary, we have analysed the dynamics of a continuously observed, driven solid state qubit, coupled to a generic bosonic environment. Both the environment and the coupling to the detector contribute to the qubit relaxation and dephasing rates. Useful spectroscopic information, in particular the dephasing rate ν_0 , can be extracted from DC measurements of the detector output current alone, even when the coupling between the microwave field and the qubit is unknown. If the power spectrum of the detector output noise can also be measured, then the relaxation rate Γ and Rabi frequency can also be determined. We have also proposed a single shot spin readout technique using microwave driving, which offers advantages over existing schemes and can be implemented with current technology.

We thank Gerard M ilburn, Charles Smith, Andrew Doherty, Jason Petta, Charlie Marcus, Bill Munro and Tim Spiller for useful conversations. SDB thanks the EU NANOMAG IQC project (IST-2001-33186) for support. TMS is funded by the CM IFUjitsu collaboration.

Electronic address: sean.barrett@hp.com

^y Electronic address: tm.s29@cam.ac.uk

- [1] R. Hanson, et al, Phys. Rev. Lett. 91, 196802 (2003); J. M. Elzerman, et al, Phys. Rev. B 67, 161308(R) (2003); S. Gardelis, et al, Phys. Rev. B 67, 073302 (2003); A. W. Rushforth, et al, Phys. Rev. B 69, 113309 (2004); L. D. Carlo, et al, Phys. Rev. Lett. 92, 226801 (2004); T. Fujisawa, et al, Nature 419, 278 (2002).
- [2] T. Hayashi, et al, Phys. Rev. Lett. 91, 226804 (2003).
- [3] J. M. Elzerman, et al, Nature 430, 431 (2004).
- [4] J. R. Petta, et al, Phys. Rev. Lett. 93, 186802 (2004).
- [5] D. Loss and D. P. DiVincenzo, Phys. Rev. A 57, 120 (1998).
- [6] T. H. Oosterkamp, et al, Nature 395 (1998).
- [7] T. Brandes, R. Aguado, and G. Platero, Phys. Rev. B 69, 205326 (2004).
- [8] S. D. Barrett and G. J. M ilburn, Phys. Rev. B 68, 155307 (2003).
- [9] K. W. Lehnert, et al, Phys. Rev. Lett. 90, 027002 (2003).
- [10] T. Duty, et al, Phys. Rev. B 69, 140503(R) (2004).
- [11] A. N. Korotkov, Phys. Rev. B 60, 5737 (1999); A. N. Korotkov and D. V. Averin, Phys. Rev. B 64, 165310 (2001); S. A. Gurvitz, Phys. Rev. B 56, 15215 (1997); S. A. Gurvitz, et al, Phys. Rev. Lett. 91, 066801 (2003); Y. Makhlin, G. Schon, and A. Shnirman, Phys. Rev. Lett. 85, 4578 (2000); S. Pilgram and M. Buttiker, Phys. Rev. Lett. 89, 200401 (2002).
- [12] H.-S. Goan, et al, Phys. Rev. B 63, 125326 (2001).
- [13] H.-S. Goan and G. J. M ilburn, Phys. Rev. B 64, 235307 (2001).
- [14] A. Y. Smimov, Phys. Rev. B 68, 134514 (2003).
- [15] C. W. Gardiner and P. Zoller, Quantum Noise (Springer, 2000).

- [16] T. M. Stace and S. D. Barrett, Phys. Rev. Lett. 92, 136802 (2004).
- [17] T. M. Stace and S. D. Barrett, cond-mat/0309610 (2003).
- [18] A. J. Leggett, et al, Rev. Mod. Phys. 59, 1 (1987).
- [19] R. Aguado and L. P. Kouwenhoven, Phys. Rev. Lett. 84, 1986 (2000).
- [20] R. J. Schoelkopf, et al, (cond-mat/0210247) (2002).
- [21] R. Blatt and P. Zoller, Eur. J. Phys. 9, 250 (1988).
- [22] H. A. Engel, et al, Phys. Rev. Lett. 93, 106804 (2004).
- [23] M. Friesen, et al, Phys. Rev. Lett. 92, 037901 (2004).
- [24] L. Vandersypen, et al, cond-mat/0407121 (2004).
- [25] S. D. Barrett and T. M. Stace, cond-mat/0411581 (2004).
- [26] This RW A implies a coarse graining in time, which means that our treatment does not describe dynamics on very short time scales of order τ^{-1} .